Agricultural and Forest Meteorology 312 (2022) 108704

Contents lists available at ScienceDirect

Agricultural and Forest Meteorology

journal homepage: www.elsevier.com/locate/agrformet

Revisiting dry season vegetation dynamics in the Amazon rainforest using different satellite vegetation datasets

Xiaoming Xie [a], Bin He [a,*], Lanlan Guo [b], Ling Huang [c], Xingming Hao [d,e], Yafeng Zhang [a], Xuebang Liu [a], Rui Tang [a], Sifan Wang [a]

[a] State Key Laboratory of Earth Surface Processes and Resource Ecology, College of Global Change and Earth System Science, Beijing Normal University, Beijing 100875, China

[b] Academy of Disaster Reduction and Emergency Management, School of Geography, Beijing Normal University, Beijing 100875, China

[c] College of Urban and Environmental Sciences, Peking University, Beijing, China

[d] State Key Laboratory of Desert and Oasis Ecology, Xinjiang Institute of Ecology and Geography, Chinese Academy of Sciences, Urumqi 830001, China

[e] Akesu National Station of Observation and Research for Oasis Agro-ecosystem, Akesu, Xinjiang 843017, China

ARTICLE INFO

Keywords:
Dry season
Vegetation data
Greening
Amazon
Rainforest

ABSTRACT

There has been a debate regarding whether the Amazon rainforest is greening during the dry season. This is partially because of the great uncertainty associated with the ability of different vegetation indices to accurately assess tropical vegetation status. This paper, revisit this issue by comprehensively examining the seasonal variations in vegetation recorded in various satellite-based vegetation datasets, namely, the leaf area index (LAI), contiguous solar-induced fluorescence (CSIF), enhanced vegetation index (EVI), and vegetation optical depth (VOD). All four of these vegetation datasets show an increase in vegetation during the dry season in most parts of the Amazon; however, the vegetation changes are not only spatially variable, but also differ among the datasets. This may be attributable in part to the different physical characteristics captured by each of the datasets. For example, the seasonal maximum value occurs first in the LAI, followed by the CSIF, EVI, and VOD, in that order. The seasonal cycle of the LAI agrees reasonably well with in-situ observations of leaf flush and leaf fall. As new leaf production offsets senescence and abscission, the dry-season vegetation increases in most parts of the Amazon rainforest. Partial correlation analysis was used to further investigate the potential climatic cues (i.e., precipitation, temperature and radiation) associated with the seasonal changes recorded in the vegetation data. We found that precipitation and radiation were the dominant potential cues for seasonal VOD (48%) and LAI (59%) changes, respectively. However, CSIF appears to be associated more closely with temperature and precipitation, with significant correlations observed across ∼x223C 37% of the Amazon rainforest area for both with CSIF. Finally, variations in the EVI showed similar sensitivity to all three climatic variables considered. The findings presented here will greatly improve our understanding of vegetation dynamics and the carbon cycle in the Amazon rainforest ecosystem.

1. Introduction

The Amazon rainforest is a huge carbon pool, accounting for ∼x223C 14% of total global net primary production (Zhao and Running, 2010). Any changes in ecosystem productivity will cause an acceleration or deceleration of the atmospheric CO_2 growth rate and ultimately trigger a feedback between the biosphere and atmosphere (Dias et al., 2002; Gash and Nobre, 1997; Wright et al., 2017; Yang et al., 2018). Both climate change and human activity have had great impacts on the stability of the Amazon rainforest ecosystem (Esquivel-Muelbert et al., 2019; Giardina et al., 2018; Gloor et al., 2015; Wagner et al., 2017). Given how critical the Amazon rainforest is to the global carbon cycle and climate change, it is urgently important to understand how a changing environment affects ecosystem processes in the region.

Currently, a clear understanding of the Amazon rainforest ecosystem is hampered by the scarcity of *in situ* observations (Atkinson et al., 2011; Lewis et al., 2011; Morton et al., 2014; Phillips et al., 2009). Satellite observations, as an alternative tool, are still the most practical way to monitor vegetation changes in large-scale regions as vast as the Amazon (Atkinson et al., 2011). However, conflicting results are frequently

* Corresponding author.
E-mail address: Hebin@bnu.edu.cn (B. He).

https://doi.org/10.1016/j.agrformet.2021.108704
Received 5 February 2021; Received in revised form 19 October 2021; Accepted 25 October 2021
Available online 3 November 2021

Table 1
Vegetation data used in this study.

Satellite vegetation data	Data products	Temporal resolution	Spatial resolution	Time series
LAI	MODIS V6	8–daily	500m	2003.1–2019.12
EVI	MAIAC-global	8–daily	0.05°	2000.1–2017.12
CSIF	Zhang (Zhang et al., 2018)	4–daily	0.05°	2000.1–2019.12
VOD	LPRM_AMSRE_D	daily	0.25°	2003.1–2010.12

obtained by different satellites and related vegetation data, triggering widely contentious debates. One of the most famous debates is whether vegetation is greening during the dry season (Doughty et al., 2019, 2021; Huete et al., 2006; Morton et al., 2014; Saleska et al., 2016). Based on the enhanced vegetation index (EVI) derived from the Moderate Resolution Imaging Spectroradiometer (MODIS), some studies argue that the increase in solar radiation during the dry season promotes vegetation photosynthetic activity, resulting in a green-up (Huete et al., 2006). However, Morton et al. (2014) suggested that this green-up is simply an artifact produced by the sun-sensor geometry of the MODIS vegetation index. With the development of satellite techniques, some new satellite observations have gradually been introduced to studies on the Amazon rainforest, such as the solar-induced chlorophyll fluorescence (SIF) product and the passive microwave-based vegetation optical depth (VOD) product (Guan et al., 2015; Liu et al., 2018). The joint use of these different satellite observations to diagnose dry-season vegetation changes may help to resolve the conflicting perspectives.

The definition of the dry season can also influence the conclusions reached regarding about vegetation changes during the dry season. Previous studies usually considered a uniform dry season over the whole Amazon rainforest (Huete et al., 2006; Morton et al., 2014; Saleska et al., 2016), ignoring the spatial differences in climatic conditions. The Amazon rainforest covers an area of more than 5 million km^2 and spans nearly 20° of latitude. Furthermore, the spatial distribution of precipitation changes with the north–south movement of the intertropical

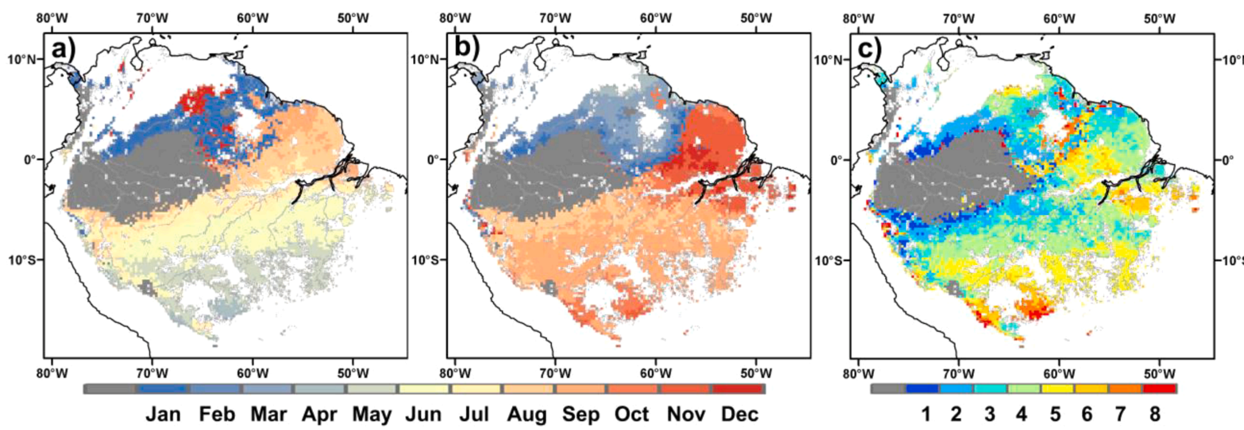

Fig. 1. Spatial pattern of the dry season across the Amazon calculated using monthly water deficits during the period 2000–2019. (a) Onset dates, (b) end dates and, and (c) length of the dry season. Gray areas indicate that rainfall is always higher than potential evapotranspiration and thus no water deficit occurred within a year. White areas are non-forest.

Table 2
In situ observations of leaf flush and leaf fall from the four stations.

ID	Site_code	Lat	Lon	leaf fall period	leaf flush period	Refs
1	K34	−2.61	−60.21	2004−2008	2012−2013	Wu et al. (2016)
2	K67	−2.86	−54.96	2001−2005	2010−2011	Wu et al. (2016)
3	Tanguro5	−13.08	−52.38	2009−2011	2009−2011	Doughty et al. (2017)
4	Keniadeep	−16.02	−62.73	2009−2011	2009−2011	Doughty et al. (2017)

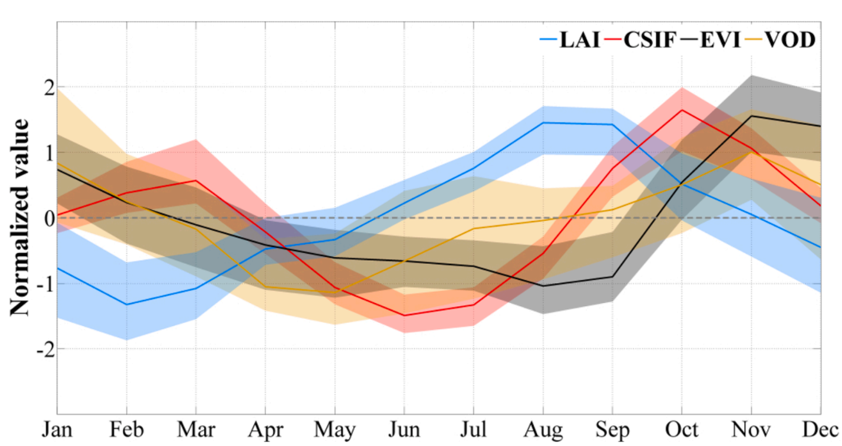

Fig. 2. Averaged seasonal cycle of LAI, CSIF, EVI and VOD in the Amazon rainforest. The shadows around the lines indicate the standard deviation.

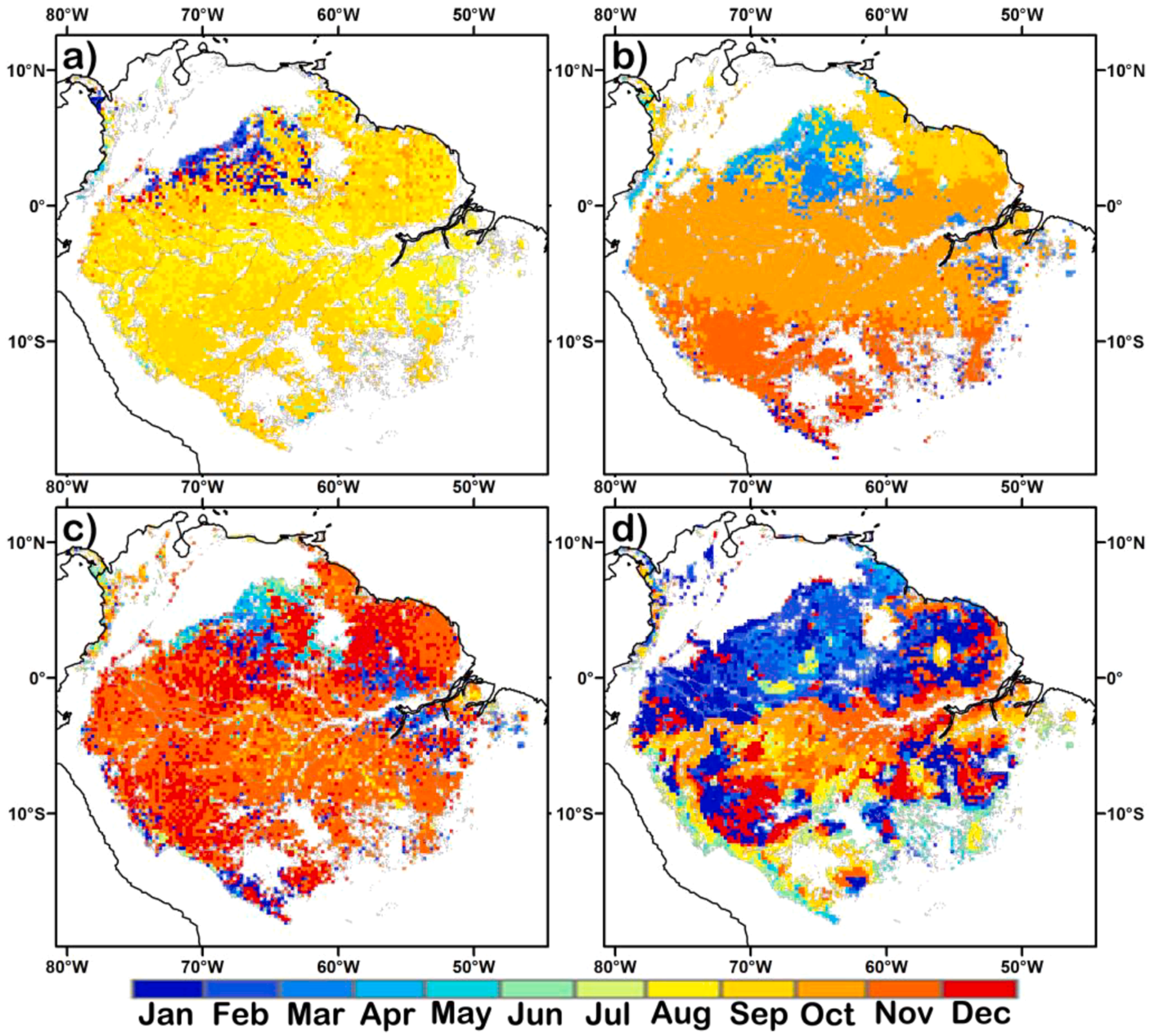

Fig. 3. Month (mean for the entire study period) when each vegetation datasets reached a maximum. (a) LAI, (b) CSIF, (c) EVI, and (d) VOD.

convergence zone. Therefore, the use of rough fixed period to define the dry season may cause a misallocation of the dry and wet seasons. Some studies have attempted to define a spatially varying dry season. For example, as the average evapotranspiration level in tropical forests is ~x223C 100 mm•month^{-1} (Anderson, 2012), the dry season has been defined as occurring when monthly precipitation falls below 100 mm (de Moura et al., 2015; Tang and Dubayah, 2017). In addition, some studies have examined the vegetation differences between the dry and wet seasons using a flexible definition of the dry season based on both precipitation and potential evaporation (Bradley et al., 2011; de Moura et al., 2015; Guan et al., 2015; Sousa et al., 2017). Clearly, to determine dry-season vegetation changes, the start and end of the dry season must first be carefully defined.

In this study, using different vegetation data retrieved from satellite observations and a spatially varying definition of the dry season, we revisited dry-season vegetation dynamics in the Amazon rainforest. The performance of various vegetation datasets are comprehensively compared and the potential climatic cues associated with each vegetation datasets are also determined.

2. Data and methodology

2.1. Data

2.1.1. Satellite-based vegetation data

Table 1 lists the vegetation data used in this study. The Leaf Area Index (LAI) is defined as the green leaf area per unit ground area (Yan et al., 2016a). The LAI product used in this study was obtained from the MODIS on Terra satellite (MOD15A2 V6). The data has an 8-day composite temporal frequency with a spatial resolution of 500 m and has been available since July 2002 (Yan et al., 2016a, 2016b). More detailed information about this dataset can be found at https://lpdaac.usgs.gov/products/mcd15a2hv006/.

The EVI measures the greenness of the vegetation canopy (Liu et al., 2018). The EVI dataset used in this study was derived from the MODIS sensor composite processed by the multiangle implementation of atmospheric correction algorithm (MAIAC) (Emili et al., 2011; Lyapustin et al., 2018, 2011). MAIAC is based on the Bidirectional Reflectance Distribution Function (BRDF) correction. It reduces the error and bias associated with view−illumination geometry, and improves the product accuracy (Bi et al., 2016; Emili et al., 2011; Wagner et al., 2017). We used observations from the Terra and Aqua satellites covering the period from 2000 to 2017 with a 0.05° spatial resolution and an 8-day temporal frequency (https://portal.nccs.nasa.gov/datashare/maiac/).

The SIF is fluorescence emitted by chlorophyll after it absorbs light

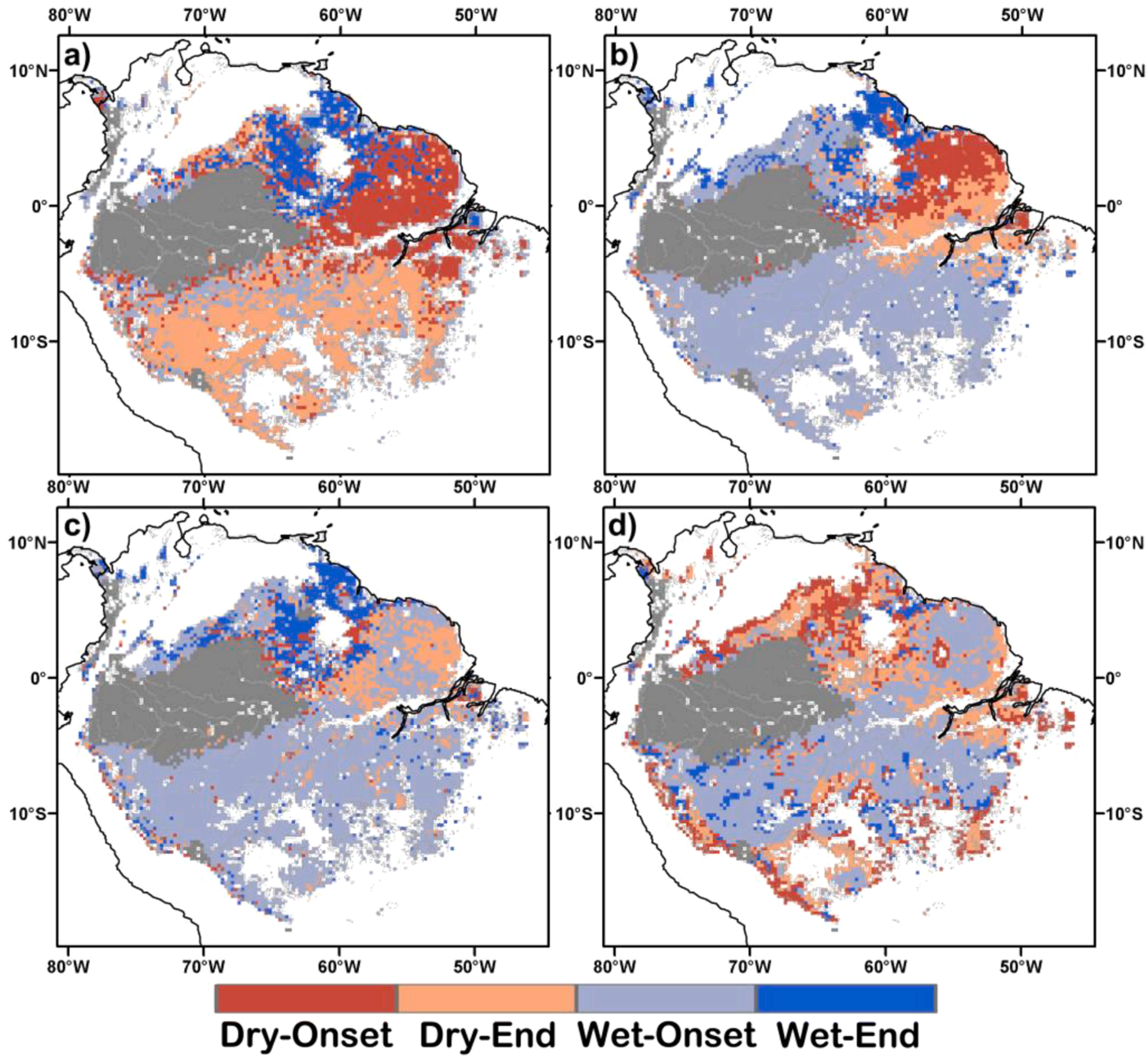

Fig. 4. Spatial distribution of the stages of the dry and wet seasons when the four vegetation datasets reached a maximum. (a) LAI, (b) CSIF, (c) EVI, and (d) VOD. Dry-Onset (Wet-Onset) is defined as when the maximum vegetation value is closer to the first month of the dry season (wet season) than the last month, whereas Dry-End (Wet-End) is defined as when the maximum vegetation value is closer to the last month of the dry season (wet season) than the first month. The gray areas were excluded from the analysis.

(Baker, 2008), and is thought to be closely related to photosynthesis and provide a diagnosis of the actual functional status of vegetation (Li et al., 2018b; Meroni et al., 2009). We used the 4-day clear-sky daily contiguous solar-induced fluorescence (CSIF; i.e., $CSIF_{clear\text{-}daily}$ which assumes no cloud throughout the day) time-series (2000–2019) with a spatial resolution of $0.05^{\circ} \times 0.05^{\circ}$from Zhang et al. (2018) (https://osf.io/8xqy6/), which measured under a clear sky to reduce the uncertainty caused by cloud. CSIF is generated based on daily OCO-2 SIF observations and the MCD43C1 C6 reflectance product, and is closely related to the temporal and spatial changes of GPP (Zhang et al., 2020, 2018). This dataset may have an advantage over GOME-2 SIF in regions strongly affected by cloud cover, particularly in the tropical rainforest (Zhang et al., 2018).

The VOD represents the total water content of vegetation (Liu et al., 2018; Walther et al., 2018). It describes the attenuation of microwave radiation emitted by the soil and the vegetation itself owing to the water contained in the canopy. The passive microwave-based VOD product with a 0.25° spatial resolution is based on the C-band (6.9 GHz) and Ka-band (36.5 GHz), which were derived from the Advanced Microwave Scanning Radiometer-Earth Observing System (AMSR-E) and processed by the Land Parameter Retrieval Model (LPRM) (Meesters et al., 2005; Owe et al., 2008). The C-band VOD measures the dynamics of water content at the canopy level (including the leaves and branches), and has no obvious sensitivity to clouds and atmospheric aerosols (Guglielmetti et al., 2007; Jones et al., 2014; Tian et al., 2016). We used daily VOD time series retrievals from night overpasses covering the period from 2003 to 2010 (Liu et al., 2018).

2.1.2. *Climate variables*

We obtained our precipitation (PRE) data from the Tropical Rainfall Measuring Mission (TRMM) V7 product (Huffman et al., 2007; Panisset et al., 2018), which provides monthly precipitation estimates spanning the area between 50°N and 50°S with a 0.25° spatial resolution. Monthly temperature (TEM) and potential evapotranspiration (PET) datasets with a 0.5° spatial resolution were obtained from the Climate Research Unit Time Series 4.03 (CRU TS4.03) (Harris et al., 2020). Additionally, monthly Photosynthetically Active Radiation (PAR) downwards data from 2000 to 2020 were derived from the Radiative Fluxes and Clouds (SYN1deg-Month Ed4A) product with a 1° spatial resolution, which is measured by the Clouds and the Earth's Radiant Energy System (CERES) instruments onboard the NASA Langley Research Center Atmosphere Science Data Center (Loeb et al., 2009). The total surface PAR was calculated as the sum of "Computed PAR Surface Flux Direct-All-sky" and "Computed PAR Surface Flux Diffuse-All-sky" (Li et al., 2018a).

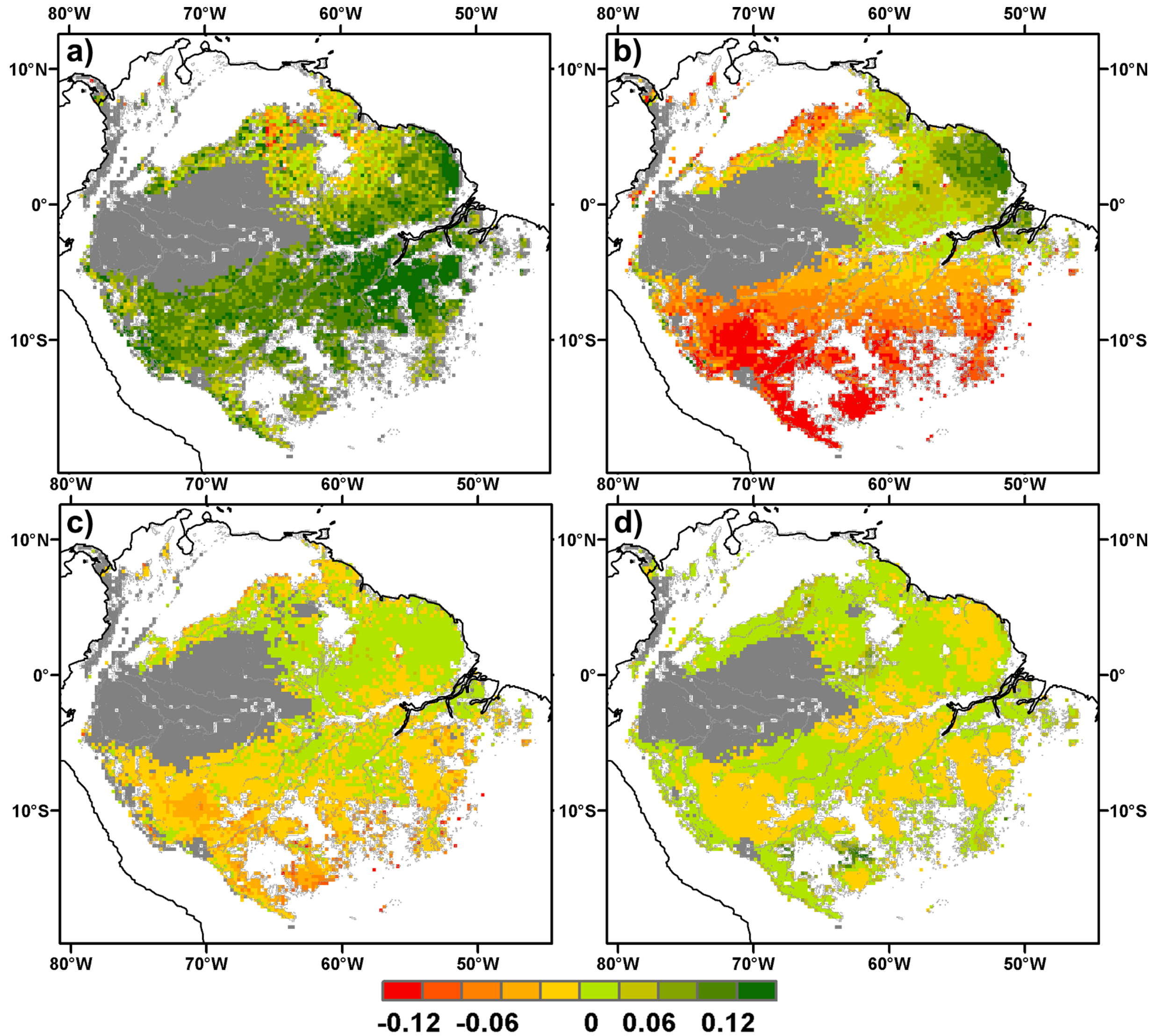

Fig. 5. Normalized dry and wet seasons differences for the four vegetation datasets (local dry season mean minus local wet season mean, divided by the sum of the two means). (a) LAI, (b) CSIF, (c) EVI, and (d) VOD. Green (red) colors indicate that the mean vegetation value during the dry season is greater (smaller) than in the wet season. The gray areas were excluded from the analysis. (For interpretation of the references to color in this figure legend, the reader is referred to the web version of this article).

We used the 0.05° MODIS land cover product (MCD12C1) from 2019, which is based on the International Geosphere-Biosphere Programme (IGBP) classification, to determine the spatial distribution of vegetation in the Amazon rainforest (Fig. 1). All pixels consisting of more than 75% forested land were considered to be forest-covered (Francesco et al., 2018).

As this study focuses on seasonal changes in vegetation, we used the original time series of vegetation data those are currently available, and converted them into monthly values. In addition, all gridded datasets were resampled onto a 0.25° grid using nearest neighbor interpolation in ArcGIS to match the spatial resolution of the satellite vegetation data to the climate variables.

2.1.3. In situ observations of forest phenology

We compiled *in situ* leaf flush and leaf fall observations from four stations from previous studies in the Amazon to evaluate the seasonal phenology of the forest (Table 2 and Fig. S1). From north to south, the sites are K34, K67, Tanguro5 and Keniadeep.

2.2. Methods

2.2.1. Identification of the dry season

We used the PRE and PET from 2000 to 2019 to define the dry season for each year. We defined the onset of the dry season as occurring when the monthly PRE value fell below the monthly PET value, and its end as when the monthly PRE exceeded the monthly PET (Guan et al., 2015). The onset, end, and duration of the dry season were determined for each pixel, and their spatial differences were explored.

2.2.2. Statistical analysis

We used partial correlation analysis to determine the climatic drivers (PRE, TEM, and PAR) of seasonal changes in the vegetation data. First, we standardized each variable (four vegetation and three climatic variables) using the mean and the standard deviation. We then used partial correlation analysis to test for the correlation between the vegetation and climatic variables. The significance of the partial correlation coefficients was evaluated at a *p*-value of $p < 0.05$.

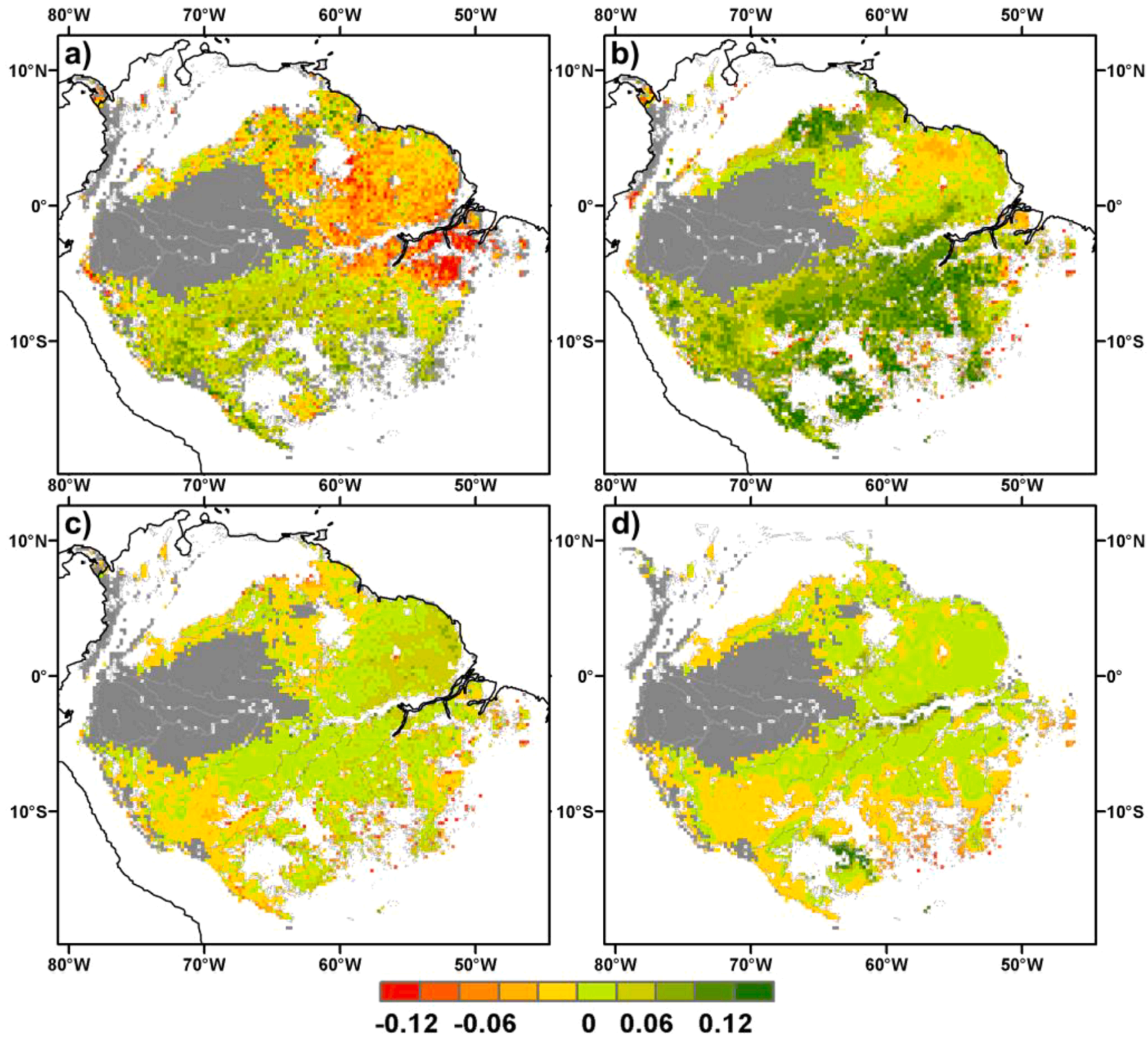

Fig. 6. Differences between the vegetation values at the end of the dry season and at the onset of the dry season (local dry season end value minus local dry season start value, divided by the sum of the two values). (a) LAI, (b) CSIF, (c) EVI, and (d) VOD. Green (red) colors indicate that the mean vegetation value at the end of the dry season is larger (smaller) than that at the onset of the dry season. The gray areas were excluded from the analysis. (For interpretation of the references to color in this figure legend, the reader is referred to the web version of this article).

3. Results

3.1. The division of the dry season

The climate of the Amazon rainforest shows great spatial differences. We found that the amplitudes of the seasonal changes, annual maxima, and annual minima of the climate variables considered here showed large spatial heterogeneity (Figs. S2 and S3). The average annual PRE varies greatly in space, ranging from less than 1000 mm in the south to more than 3000 mm in the northwest (Fig. S4a). There is a relatively large average annual PET in the south and north compared with the central areas (Fig. S4b). This suggests that the use of a uniform definition of the dry season over the whole Amazon rainforest may be inappropriate.

Fig. 1 shows the spatial pattern of the dry season when defined as when PRE < PET. The gray areas where PRE was always higher than PET were excluded from our analysis. Widespread spatial differences in the onset, end date, and length of the dry season over the Amazon rainforest are evident. The onset and end date of the dry season generally increases from the southwest to the northeast following the PRE gradient (Carlos, 1977). The onset of the dry season occurs mainly between May and June, and it ends between September and October over the southwest, indicating that there are about four to five months of water deficit. In the central−east area, the onset of the dry season occurs between August and September and ends between November and December. In the extreme north, near the equator, the dry season lasts only about two to three months, with the start of the dry season occurring between March and October, and the end between April and the following February.

3.2. Seasonal cycle of four vegetation variables

To gain an insight into the differences among the four vegetation datasets during the dry season, we first explored their seasonal cycles across the Amazon rainforest (Fig. 2). Apart from the LAI, the other three vegetation datasets generally follow a consistent seasonal cycle across the study region as a whole. The LAI shows higher values from July to September and lower values from January to March. The CSIF, EVI, and VOD are similar to each other but lag the LAI by about three to four months.

The spatial distribution of the maximum values of the LAI, CSIF, and EVI agree reasonably well with the peak of their respective seasonal cycles (Fig. 3). The maximum LAI occurs mainly in August or September, and the maximum CSIF occurs in October and November, one month ahead of the maximum EVI. The gradient of the maximum VOD is

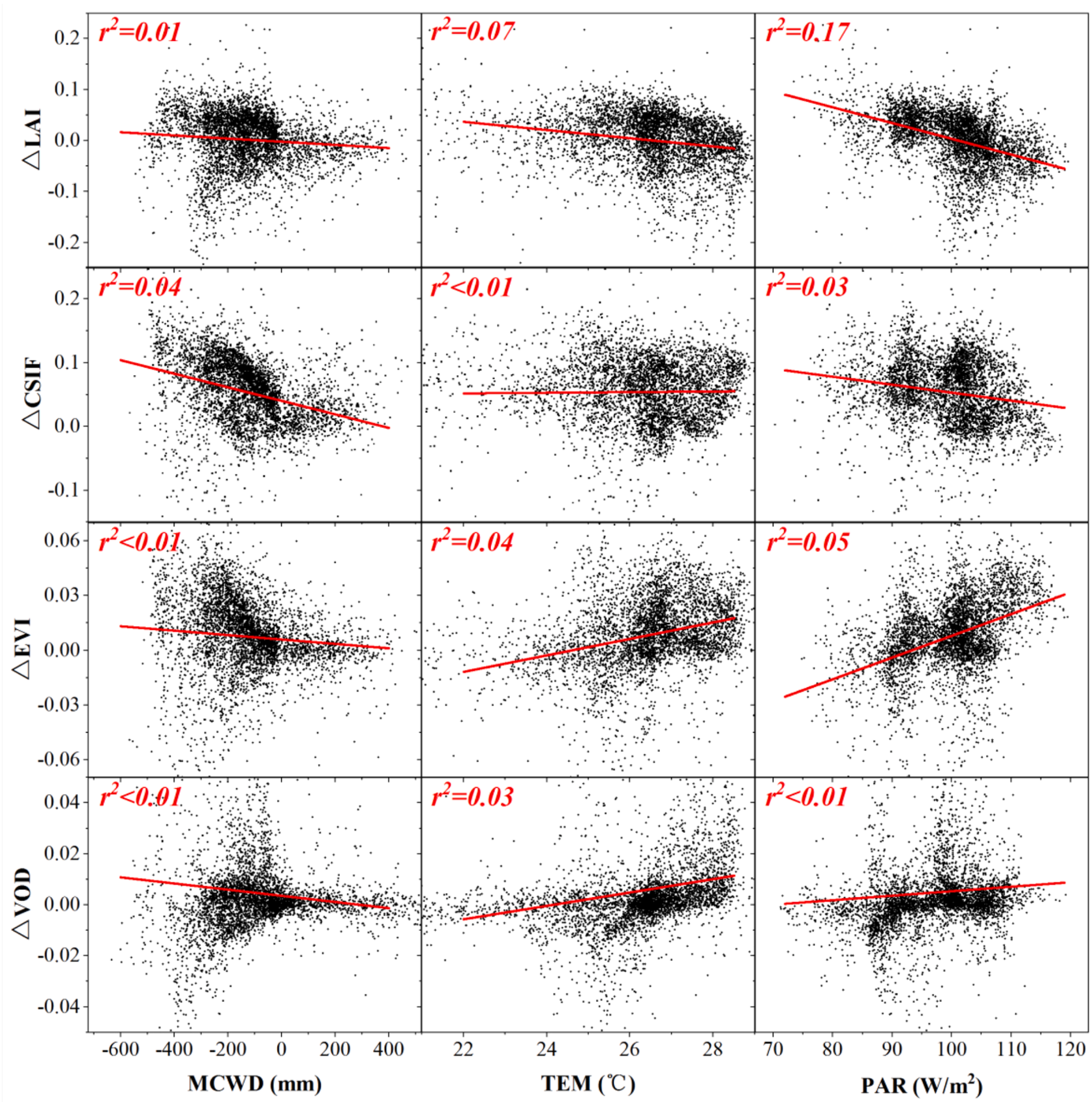

Fig. 7. Relationship between the change in the four vegetation datasets (values at the end of the dry season minus those at the onset of the dry season, denoted as ΔLAI, ΔCSIF, ΔEVI and ΔVOD) during the dry season and MCWD, mean TEM and mean PAR. The red line was determined using an ordinary least-squares model. All correlations are significant at $p< 0.5$.

directed from south to north, with the maximum in the south occurring between August and September, the maximum in the central Amazon occurring between November and January, and the maximum in the north occurring between January and February. The minimum LAI occurs in January or February over most of the Amazon rainforest, except in the north where it occurs between May and July (Fig. S5). The minimum CSIF occurs between May and July, one month ahead of the minimum EVI. The minimum VOD also has a southwest−northeast gradient and precedes the maximum VOD by six months.

We further classified the dry and wet seasons into four periods (Dry-Onset, Dry-End, Wet-Onset and Wet-End) to determine the time of occurrence of the maximum and minimum values of the four vegetation datasets, as shown in Figs. 4 and S6. In the south of the Amazon rainforest, the maximum LAI occurs predominantly during the Dry-End period (39% of the total area). In the northeast and northern regions, the maximum LAI appears during the Dry-Onset period (26% of the total area) and during the Wet-End period (13% of the total area), respectively. In the south, the CSIF reaches a maximum during the Wet-Onset period in 63% of the total area, later than the LAI. The CSIF maxima during the Dry-Onset and Dry-End periods are distributed mainly in the northeast Amazon rainforest, whereas the maximum during the Wet-End period occurs mainly in parts of the northern Amazon. For the EVI and VOD, the peak occurs during the Wet-Onset period in almost the entire Amazon rainforest (68% and 48% of the total area, respectively). On the other hand, the minimum LAI, CSIF, EVI, and VOD all occur primarily during the Wet period (94%, 50%, 68%, and 84% of the total area, respectively).

3.3. *Vegetation dynamics indicated by different satellite vegetation data during the dry and wet seasons*

We now compare the performance in demonstrating the vegetation changes between the wet and dry seasons based on the four vegetation datasets. We calculated the dry to wet difference of each vegetation datasets as the mean vegetation datasets value during the dry season minus the mean vegetation datasets value during the wet season, and then normalized the results (using the local dry season mean minus the local wet season mean, divided by the sum of the two means). The

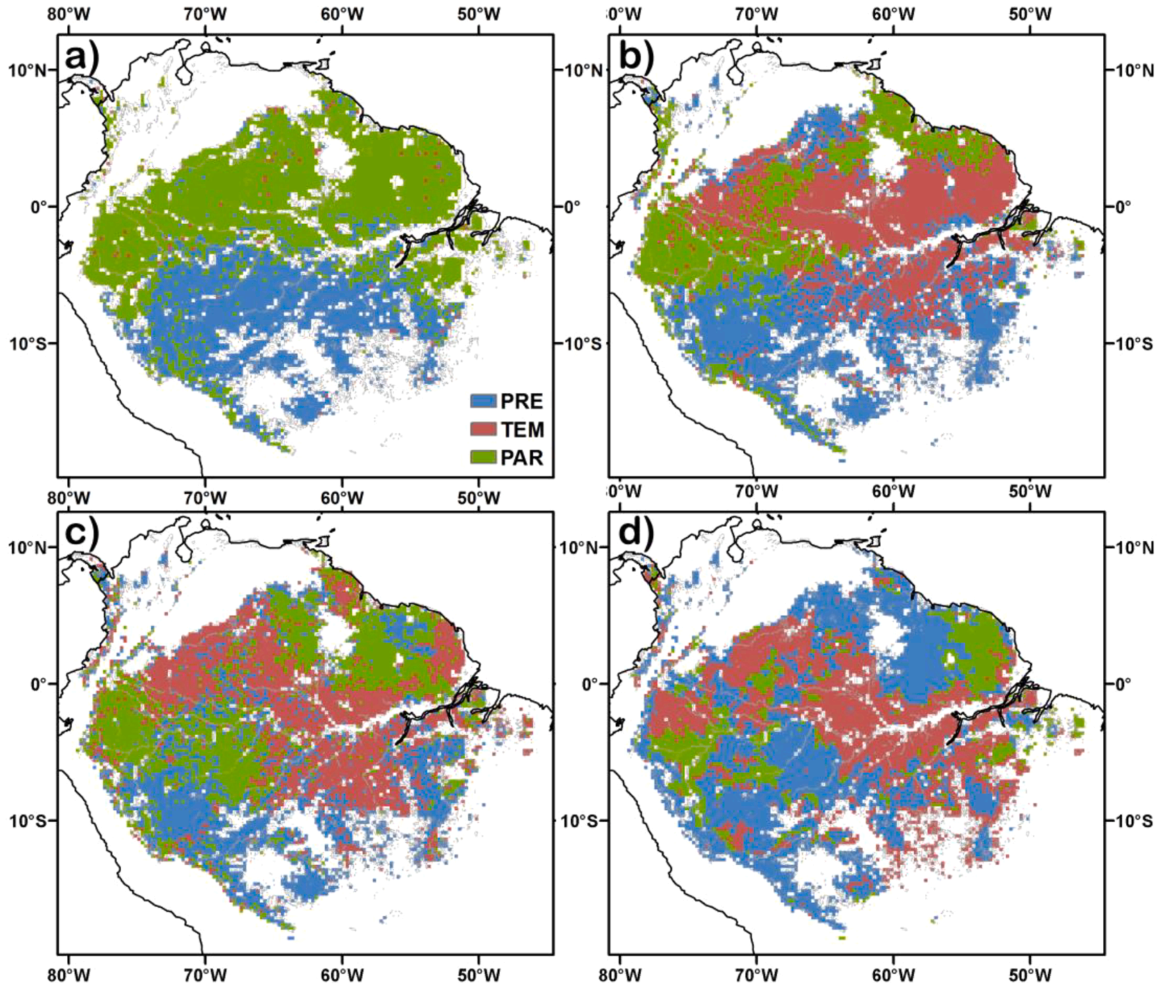

Fig. 8. RGB composite of the sensitivity of the seasonal changes in four vegetation datasets to PRE, TEM, and PAR. (a) LAI, (b) CSIF, (c) EVI, and (d) VOD. Blue, red, and green colors indicate PRE, TEM, and PAR sensitivity, respectively. (For interpretation of the references to color in this figure legend, the reader is referred to the web version of this article).

Amazon rainforest shows a more prevalent increase in the LAI during the dry season than the wet season, except for a fraction of the northern region (Fig. 5a). The CSIF and EVI show similar patterns to each other (Fig. 5b, c), with larger values during the dry season than the wet season in the northeast, and vice versa in the south of the Amazon. For the majority of regions, the VOD is larger in the dry season than in the wet season, particularly in the northern part of the Amazon (Fig. 5d).

Next, we assessed the vegetation dynamics for the dry season using the values of the four vegetation datasets during the end period minus those during onset date of dry season (Fig. 6). Overall, all four vegetation datasets show an increase during the dry season in most parts of the Amazon rainforest; however, the spatial patterns are not consistent. During the dry season, the LAI, CSIF, EVI, and VOD increase over 71%, 89%, 77%, and 74% of the total Amazon rainforest area, respectively. The LAI decreases during the dry season in the northeast of the Amazon, but an increasing trend is observed in the south (Fig. 6a). The CSIF also increases during the dry season in the south of the Amazon, but decreases in the northeast over a much smaller area than the LAI. The spatial patterns of the EVI and VOD during the dry season differ from those of the LAI and CSIF: decreases are observed in the southwestern Amazon, while weak increases are found in the southeastern and northern Amazon.

3.4. Potential climatic cues for vegetation changes during the dry season

The seasonal variation of vegetation is affected mainly by climate variables (e.g. precipitation and insolation) in the Amazon (Wagner et al., 2017). To investigate the potential climatic cues for vegetation variability during the dry season, we researched the relationship between the change in the four vegetation datasets (values at the end of the dry season minus those at the onset of the dry season, denoted as ΔLAI, ΔCSIF, ΔEVI and ΔVOD) and the cumulative water deficit (MCWD), mean TEM and mean PAR of the dry season (Fig. 7). During the dry season, the four vegetation datasets all decreased with increasing MCWD. ΔLAI and ΔCSIF had a negative correlation with mean TEM and mean PAR, and the stronger relationship occurring with mean PAR. This implies that ΔLAI and ΔCSIF decreased despite higher solar radiation during the dry season. In contrast, ΔEVI and ΔVOD had positive relationships with mean TEM and mean PAR. These results indicate that the four vegetation datasets have different responses to PRE, TEM, and PAR during the dry season.

The response of the seasonal changes in the four vegetation datasets to PRE, TEM, and PAR was investigated further using partial correlation analysis (Fig. 8). We found that the seasonal changes in the LAI are related to PAR in 59% of the total area of the Amazon rainforest. The southern regions are most relevant to variations in PRE, whereas lower-latitude areas exhibit stronger responses to PAR. The seasonal CSIF changes exhibit a stronger relationship with TEM and PRE than to PAR, mainly near the equator. In the north of the Amazon, the CSIF demonstrates a strong relationship with PAR, accounting for 25% of the Amazon rainforest area. The relationship of the EVI with PRE, TEM, and PAR is more or less equally split across the Amazon, accounting for 33%,

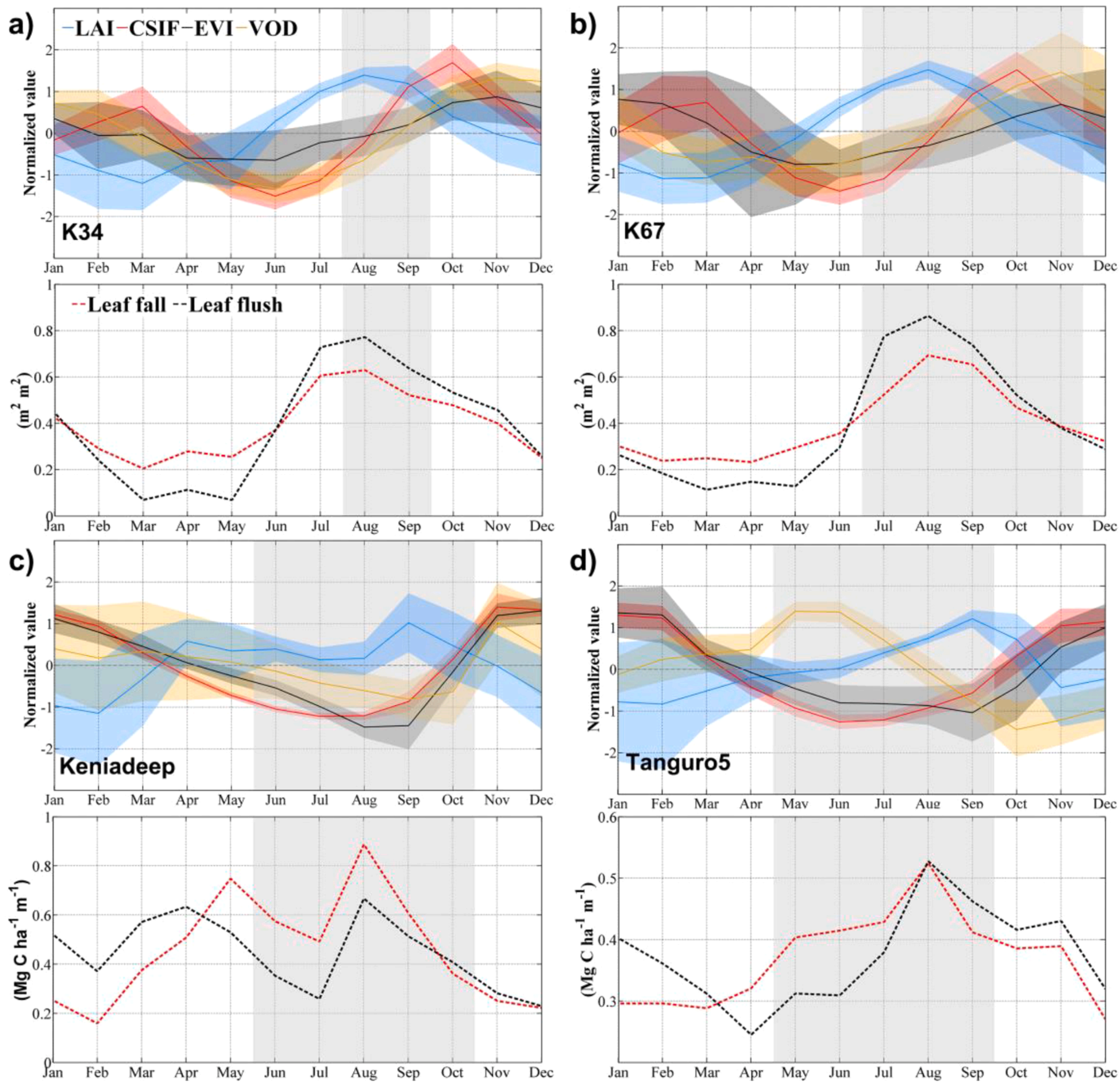

Fig. 9. Seasonal cycle of each vegetation datasets against *in situ* observed leaf flush and leaf fall in the Amazon rainforest. The gray highlighted areas indicate the dry season.

36%, and 31% of the total area, respectively. The VOD is most relevant to PRE, covering 48% of the total area, followed by TEM in 36% of the Amazon and PAR in 16%.

4. Discussion

This study used four different satellite-based vegetation datasets to explore whether vegetation is greening during the dry season and aimed to quantify the potential climatic cues for vegetation productivity using partial correlation analysis. Various studies have noted that spatial patterns of vegetation change coincide with the onset date of the dry season, which generally progresses from southwest to northeast (Myneni et al., 2007). However, our results demonstrate that the vegetation changes are not only spatially different, but also differ among the four vegetation datasets throughout the dry season (Figs. 5 and 6). This differs from when vegetation changes are determined using the classic definition of the dry season which does not consider spatial differences (Figs S7 and 8). Furthermore, in terms of the dynamic changes to vegetation during the dry season, several vegetation datasets increase in most parts of Amazon. This is broadly consistent with the findings from previous investigations (Huete et al., 2006; Saleska et al., 2016). A possible explanation is that the understory vegetation is more strongly related to the seasonal structural dynamics of the canopy layer than to precipitation or insolation, and hence the greening of the canopy during the early dry season and the subsequent loss of the canopy is partly offset by the increase in the LAI in the understory during the late dry season (Tang and Dubayah, 2017). Another explanation is that plant water storage buffers the seasonal dynamics of water supply and demand, and sustains fresh leaves formed during the dry season (Feng et al., 2018).

The reasons for the differences between the four vegetation datasets during the dry season may be attributable in part to the different physical characteristics that they capture (Janssen et al., 2021). Therefore, we used four *in situ* forest phenology observations to investigate the seasonal variation of the satellite-based vegetation data with leaf flush and leaf fall (Fig. 9). The seasonal trends in leaf flush and leaf fall follow each other fairly well at the four sites, and both leaf flush and leaf fall peaks occur during the dry season. This is consistent with previous findings that leaf flush and leaf fall are relatively high in May–September, relatively low in January–April, and peak in August (Restrepo-Coupe et al., 2013; Wu et al., 2016). At these sites, the peak LAI occurs when leaf flush and leaf fall are at a maximum, and the maximum LAI values occur during the dry season. This could be interpreted as that the synchronization of new leaf growth with dry season leaf fall shifts the canopy composition toward younger, more light-use efficient leaves

(Wu et al., 2016). Consequently, the canopies develop younger leaves, which have higher stomatal conductance and biochemical parameters needed for photosynthesis than older leaves (Albert et al., 2018; Doughty and Goulden, 2008; Kim et al., 2012; Wu et al., 2016), leading to the greening of vegetation during the dry season. The highest production of leaf flush and leaf fall occurs ahead of the peaks in CSIF and EVI. The SIF is the energy emitted by plant chlorophyll molecules (Müller, 1874). The period required for new leaves to reach maturity is about one month, after which they quickly reach the peak of photosynthesis (Restrepo-Coupe et al., 2013; Sobrado, 1994). When they do, the CSIF also reaches its peak. Previous studies have suggested that the EVI lags the SIF by approximately one month (Walther et al., 2016). This may be because photosynthesis of chlorophyll reaches its peak after the leaves enter their fastest growth stage (Walther et al., 2016). The VOD significantly lags the seasonal variation shown by the other vegetation datasets. This may be supported by the findings of Jones et al. (2012), who showed that the VOD, which represents the above ground biomass and water content, requires some time to accumulate and grow. In addition, uncertainties in the satellite observations caused by cloud cover are unavoidable factors that may also have affected our results.

Previous studies have demonstrated that the seasonal variation of vegetation in the Amazon is significantly affected by climatic variables (Wagner et al., 2017). This study has further quantified the potential climatic cues for the four different vegetation datasets using partial correlation analysis. All four vegetation data indicate that the vegetation of in the southern Amazon seems to mainly depend on the water stress (Guan et al., 2015). In contrast, the vegetation datasets in the northern Amazon shows a vegetation increase, suggesting that the vegetation in these regions can maintain photosynthetic activity during the dry season. This may be because the vegetation in drier areas is limited by the available water, whereas TEM and PAR effect leaf growth in the wetter regions (Myneni et al., 2007;(Silva et al., 2013) Silva, 2013; Wagner, 2017). This finding was also reported by Bertani et al. (2017) who explored the seasonal response of photosynthetic activity to PAR and PRE. However, their study did not consider temperature, so that solar radiation explained most areas of the Amazon rainforest. Our results also showed that different vegetation datasets show significantly different responses to climatic variables. For example, compared with other vegetation datasets, the LAI and the VOD are more strongly affected by water limitation than by TEM or PAR, whereas the CSIF is more sensitive to TEM and PRE. In addition, the sensitivity of the EVI to PRE, TEM, and PAR is consistent.

5. Conclusions

In this investigation, we have revisited the issue of how vegetation changes in the Amazon rainforest during the dry season and discussed the potential climatic cues associated with the spatial differences in four vegetation datasets. We have shown that the onset date and length of the dry season varies greatly across the Amazon. All four vegetation datasets considered show an increase during the dry season in most parts of the Amazon rainforest, but their sensitivity to the dry season show well-defined spatial differences. These differences are caused primarily by the temporal and spatial differences in the PRE, TEM, and PAR, and by different types of vegetation having different relationships with these climatic variables. Moreover, the spatial differences are further exacerbated because the four vegetation datasets all reflect different physical processes. These findings have significant implications for the understanding of seasonal changes in ecosystem processes across the Amazon rainforest under a changing climate.

Declaration of Competing Interest

We declare that we have no financial and personal relationships with other people or organizations that can inappropriately influence our work, there is no professional or other personal interest of any nature or kind in any product, service and/or company that could be construed as influencing the position presented in, or the review of, the manuscript entitled.

Acknowledgments

The authors declare that they have no conflict of interest. This work was financially supported by the Cross Team Project of the "Light of West China" Program of Chinese Academy of Sciences (No: E0284101), the National Key Research and Development Program of China (Grant no. 2017YFA0603601), and the Strategic Priority Research Program of the Chinese Academy of Sciences (Grant No. XDA20060402).

Supplementary materials

Supplementary material associated with this article can be found, in the online version, at doi:10.1016/j.agrformet.2021.108704.

References

Albert, L.P., et al., 2018. Age-dependent leaf physiology and consequences for crown-scale carbon uptake during the dry season in an Amazon evergreen forest. New Phytol. 219 (3), 870–874.

Anderson, L.O., 2012. Biome-scale forest properties in Amazonia based on field and satellite observations. Remote Sens. 4 (5), 1245–1271 (Basel).

Atkinson, P., Dash, J., Jeganathan, C., 2011. Amazon vegetation greenness as measured by satellite sensors over the last decade. Geophys. Res. Lett. 38 (19), 1–6.

Baker, N.R., 2008. Chlorophyll fluorescence: a probe of photosynthesis in vivo. Annu. Rev. Plant Biol. 59 (1), 89–113.

Bertani, G., Wagner, F.H., Anderson, L.O., Aragão, L.E.O.C., 2017. Chlorophyll fluorescence data reveals climate-related photosynthesis seasonality in Amazonian forests. Remote Sens. 9 (12), 1275 (Basel).

Bi, J., et al., 2016. Amazon forests' response to droughts: a perspective from the MAIAC product. Remote Sens. 8 (4), 356 (Basel).

Bradley, A.V., et al., 2011. Relationships between phenology, radiation and precipitation in the Amazon region. Glob. Change Biol. 17 (6), 2245–2260.

Carlos, Goldenberg, et al., Fundagao instituto, Brasileiro de geografia e estatistica, Diretoria tecnica, 1977. Plant community in Amazon forest. Geography of Brazil. Sergraf-IBGE, Rio de Janeiro, pp. 63–66.

de Moura, Y.M., et al., 2015. Seasonality and drought effects of Amazonian forests observed from multi-angle satellite data. Remote Sens. Environ. 171, 278–290.

Dias, M.S., et al., 2002. Cloud and rain processes in a biosphere-atmosphere interaction context in the Amazon region. J. Geophys. Res. Atmos. 107 (D20), 8072. LBA 39-18.

Doughty, C.E., Goulden, M.L., 2008. Seasonal patterns of tropical forest leaf area index and CO_2 exchange. J. Geophys. Res. Biogeosci. 113 (G1), G00B06.

Doughty, C.E., et al., 2017. Can leaf spectroscopy predict leaf and forest traits along a Peruvian tropical forest elevation gradient? J. Geophys. Res. Biogeosci. 122 (11), 2952–2965.

Doughty, R., Khler, P., Frankenberg, C., Magne Y, T.S, Moore, B., 2019. TROPOMI reveals dry-season increase of solar-induced chlorophyll fluorescence in the Amazon forest. Proc. Nat. Acad. Sci. 116 (44), 22393–22398.

Doughty, R., Xiao, X., Qin, Y., Wu, X., Moore, B., 2021. Small anomalies in dry-season greenness and chlorophyll fluorescence for Amazon moist tropical forests during El Nio and La Nia. Remote Sens. Environ. 253, 112196.

Emili, E., et al., 2011. High spatial resolution aerosol retrieval with MAIAC: application to mountain regions. J. Geophys. Res. Atmos. 116 (D23).

Esquivel-Muelbert, A., et al., 2019. Compositional response of Amazon forests to climate change. Glob. Change Biol. 25 (1), 39–56.

Feng, T., et al., 2018. Coupling of ecosystem-scale plant water storage and leaf phenology observed by satellite. Nat. Ecol. Evolut. 2 (9), 1428–1435.

Francesco, et al., 2018. Tall Amazonian forests are less sensitive to precipitation variability. Nat. Geosci.

Gash, J., Nobre, C., 1997. Climatic effects of Amazonian deforestation: some results from ABRACOS. Bull. Am. Meteorol. Soc. 78 (5), 823–830.

Giardina, F., et al., 2018. Tall Amazonian forests are less sensitive to precipitation variability. Nat. Geosci. 11 (6), 405–409.

Gloor, M., et al., 2015. Recent Amazon climate as background for possible ongoing and future changes of Amazon humid forests. Glob. Biogeochem. Cycl. 29 (9), 1384–1399.

Guan, K., et al., 2015. Photosynthetic seasonality of global tropical forests constrained by hydroclimate. Nat. Geosci. 8 (4), 284–289.

Guglielmetti, M., et al., 2007. Measured microwave radiative transfer properties of a deciduous forest canopy. Remote Sens. Environ. 109 (4), 523–532.

Harris, I., Osborn, T.J., Jones, P., Lister, D., 2020. Version 4 of the CRU TS monthly high-resolution gridded multivariate climate dataset. Sci. Data 7 (1).

Huete, A.R., et al., 2006. Amazon rainforests green-up with sunlight in dry season. Geophys. Res. Lett. 33 (6).

Huffman, G.J., et al., 2007. The TRMM multisatellite precipitation analysis (TMPA): quasi-global, multiyear, combined-sensor precipitation estimates at fine scales. J. Hydrometeorol. 8 (1), 38–55.

Janssen, T.A., Velde, Y., Hofhansl, F., Luyssaert, S., Han, A., 2021. Drought effects on leaf fall, leaf flushing and stem growth in Neotropical forest; reconciling remote sensing data and field observations. Biogeosciences 18 (14), 4445–4472.
Jones, M.O., Kimball, J.S., Jones, L.A., McDonald, K.C., 2012. Satellite passive microwave detection of North America start of season. Remote Sens. Environ. 123, 324–333.
Jones, M.O., Kimball, J.S., Nemani, R.R., 2014. Asynchronous Amazon forest canopy phenology indicates adaptation to both water and light availability. Environ. Res. Lett. 9 (12), 124021.
Kim, Y., et al., 2012. Seasonal carbon dynamics and water fluxes in an a mazon rainforest. Glob. Change Biol. 18 (4), 1322–1334.
Lewis, S.L., Brando, P.M., Phillips, O.L., van der Heijden, G.M., Nepstad, D., 2011. The 2010 amazon drought. Science 331 (6017), 554.
Li, X., Xiao, J., He, B., 2018a. Higher absorbed solar radiation partly offset the negative effects of water stress on the photosynthesis of Amazon forests during the 2015 drought. Environ. Res. Lett. 13 (4), 044005.
Li, X., Xiao, J.F., He, B.B., 2018b. Chlorophyll fluorescence observed by OCO-2 is strongly related to gross primary productivity estimated from flux towers in temperate forests. Remote Sens. Environ. 204, 659–671.
Liu, Y.Y., et al., 2018. Enhanced canopy growth precedes senescence in 2005 and 2010 Amazonian droughts. Remote Sens. Environ. 211, 26–37.
Loeb, N.G., et al., 2009. Toward optimal closure of the Earth's top-of-atmosphere radiation budget. J. Clim. 22 (3), 748–766.
Lyapustin, A., Wang, Y., Korkin, S., Huang, D., 2018. MODIS Collection 6 MAIAC algorithm. Atmos. Meas. Tech. 11 (10), 5741–5765.
Lyapustin, A., et al., 2011. Multiangle implementation of atmospheric correction (MAIAC): 2. Aerosol algorithm. J. Geophys. Res. Atmos. 116 (D3).
Meesters, A.G., De Jeu, R.A., Owe, M., 2005. Analytical derivation of the vegetation optical depth from the microwave polarization difference index. IEEE Geosci. Remote Sens. Lett. 2 (2), 121–123.
Meroni, M., et al., 2009. Remote sensing of solar-induced chlorophyll fluorescence: review of methods and applications. Remote Sens. Environ. 113 (10), 2037–2051.
Morton, D.C., et al., 2014. Amazon forests maintain consistent canopy structure and greenness during the dry season. Nature 506 (7487), 221–224.
Müller, N.J.C., 1874. Untersuchungen über die diffusion der atmosphärischen gase und die gasausscheidung unter verschiedenen beleuchtungs-bedingungen. Jahrb. Wiss. Botanik 9, 13.
Myneni, R.B., et al., 2007. Large seasonal swings in leaf area of Amazon rainforests. Proc. Nat. Acad. Sci. 104 (12), 4820–4823.
Owe, M., de Jeu, R., Holmes, T., 2008. Multisensor historical climatology of satellite-derived global land surface moisture. J. Geophys. Res. Earth Surf. 113 (F1).
Panisset, J.S., et al., 2018. Contrasting patterns of the extreme drought episodes of 2005, 2010 and 2015 in the Amazon basin. Int. J. Climatol. 38 (2), 1096–1104.
Phillips, O.L., et al., 2009. Drought sensitivity of the Amazon rainforest. Science 323 (5919), 1344–1347.
Restrepo-Coupe, N., et al., 2013. What drives the seasonality of photosynthesis across the Amazon basin? A cross-site analysis of eddy flux tower measurements from the Brasil flux network. Agric. For. Meteorol. 182, 128–144.
Saleska, S.R., et al., 2016. Dry-season greening of Amazon forests. Nature 531 (7594), E4–E5.
Silva, Fabrício B, Shimabukuro, Yosio E, Aragão, Luiz E.O.C., Anderson, Liana O., et al., 2013. Large-scale Heterogeneity of Amazonian Phenology Revealed from 26-year Long AVHRR/NDVI Time-series. Environmental Research Letters 8 (2).
Sobrado, M., 1994. Leaf age effects on photosynthetic rate, transpiration rate and nitrogen content in a tropical dry forest. Physiol. Plant. 90 (1), 210–215.
Sousa, D., et al., 2017. Progress in remote sensing of photosynthetic activity over the amazon basin. Remote Sens. 9 (9).
Tang, H., Dubayah, R., 2017. Light-driven growth in Amazon evergreen forests explained by seasonal variations of vertical canopy structure. Proc. Nat. Acad. Sci. 114 (10), 2640–2644.
Tian, F., et al., 2016. Remote sensing of vegetation dynamics in drylands: evaluating vegetation optical depth (VOD) using AVHRR NDVI and *in situ* green biomass data over West African Sahel. Remote Sens. Environ. 177, 265–276.
Wagner, F.H., et al., 2017. Climate drivers of the Amazon forest greening. PLoS ONE 12 (7).
Walther, S., et al., 2018. Assessing the dynamics of vegetation productivity in circumpolar regions with different satellite indicators of greenness and photosynthesis. Biogeosciences 15 (20), 6221–6256.
Walther, S., et al., 2016. Satellite chlorophyll fluorescence measurements reveal large-scale decoupling of photosynthesis and greenness dynamics in boreal evergreen forests. Glob. Change Biol. 22 (9), 2979–2996.
Wright, J.S., et al., 2017. Rainforest-initiated wet season onset over the southern Amazon. Proc. Nat. Acad. Sci. 114 (32), 8481–8486.
Wu, J., et al., 2016. Leaf development and demography explain photosynthetic seasonality in Amazon evergreen forests. Science 351 (6276), 972–976.
Yan, K., et al., 2016a. Evaluation of MODIS LAI/FPAR product collection 6. Part 1: consistency and improvements. Remote Sens. 8 (5), 359 (Basel).
Yan, K., et al., 2016b. Evaluation of MODIS LAI/FPAR product collection 6. Part 2: validation and intercomparison. Remote Sens. 8 (6), 460 (Basel).
Yang, Y., et al., 2018. Post-drought decline of the Amazon carbon sink. Nat. Commun. 9 (1), 1–9.
Zhang, Y., Commane, R., Zhou, S., Williams, A.P., Gentine, P., 2020. Light limitation regulates the response of autumn terrestrial carbon uptake to warming. Nat. Clim. Change 1–5.
Zhang, Y., Joiner, J., Alemohammad, S.H., Sha, Z., Gentine, P., 2018. A global spatially contiguous solar-induced fluorescence (CSIF) dataset using neural networks. Biogeosciences 15 (19), 5779–5800.
Zhao, M., Running, S.W., 2010. Drought-induced reduction in global terrestrial net primary production from 2000 through 2009. Science 329 (5994), 940–943.